Accepted Manuscript

The coupling effects of laser thermal shock and surface nitridation on mechanical properties of Zr-based metallic glass

Hu Huang, Minqiang Jiang, Jiwang Yan

PII: S0925-8388(18)33076-7

DOI: 10.1016/j.jallcom.2018.08.195

Reference: JALCOM 47283

To appear in: *Journal of Alloys and Compounds*

Received Date: 21 June 2018

Revised Date: 30 July 2018

Accepted Date: 20 August 2018

Please cite this article as: H. Huang, M. Jiang, J. Yan, The coupling effects of laser thermal shock and surface nitridation on mechanical properties of Zr-based metallic glass, *Journal of Alloys and Compounds* (2018), doi: 10.1016/j.jallcom.2018.08.195.

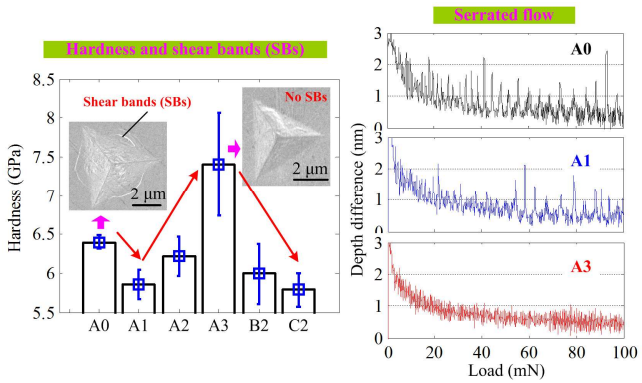

The coupling effects of laser thermal shock and surface nitridation on mechanical properties of Zr-based metallic glass

Hu Huang[a,b,*], Minqiang Jiang[c,d], and Jiwang Yan[b,*]

[a]*School of Mechanical Science and Engineering, Jilin University, Changchun, Jilin, 130022, China*

[b]*Department of Mechanical Engineering, Faculty of Science and Technology, Keio University, Yokohama 223-8522, Japan*

[c]*State Key Laboratory of Nonlinear Mechanics, Institute of Mechanics, Chinese Academy of Sciences, Beijing 100190, People's Republic of China*

[d]*School of Engineering Science, University of Chinese Academy of Sciences, Beijing 100049, PR China*

Abstract

Laser processing is a versatile tool for applications in the field of metallic glasses (MGs). Previous studies reported that surface nitridation, i.e. the formation of ZrN phase, occurred when laser irradiation of Zr-based MG was performed in nitrogen gas. Additionally, it was reported that laser thermal shock usually softened the irradiated surface. Therefore, the coupling effects of laser thermal shock and surface nitridation on mechanical characteristics of Zr-based MG should be further clarified. For this purpose, in this study, laser irradiation of Zr-based MG was conducted under various experimental conditions, followed by evaluating the surface characteristics by X-ray diffraction (XRD), nanoindentation, and energy-dispersive X-ray (EDX) spectroscopy. Experimental results indicated that the nanoindentation hardness, serrated flow, and surface shear bands were significantly affected by laser irradiation in nitrogen gas. Both surface softening and hardening were observed which depended on the experimental conditions. A competition mechanism between laser thermal shock and the introduction of ZrN phase was employed to

* Corresponding author. E-mail address: huanghu@jlu.edu.cn; yan@mech.keio.ac.jp.

rationalize these results. Furthermore, the affecting layer of ZrN phase along the depth direction was measured by EDX. The obtained results suggest a new method to introduce secondary phase into Zr-based MG surface and further to tune the mechanical characteristics of MGs.

Keywords: metallic glass; laser irradiation; surface nitridation; hardness; serrated flow; shear band

1. Introduction

Metallic glasses (MGs) with an amorphous atomic structure show unique mechanical, physical, and chemical properties compared to their crystalline counterparts, such as high hardness, strength, elasticity, good resistance to wear and chemical corrosion [1, 2]. Accordingly, they are promising structural and functional materials for potential applications in spacecrafts, molds, precision instruments, sport products, electronic frames, medical implants, and so on [3-5]. However, their practical applications are greatly hindered due to (1) size limitation and (2) very limited tensile plasticity of most MGs.

To solve these two critical problems, various preparation and processing methods have been proposed [6-10]. Laser processing as a versatile method has been applied in the field of MGs, providing unique solutions for some problems that hinder the application of MGs [11-17]. For example, laser welding of small MGs was attempted to enlarge the product size of MGs, by which Ti-based, Pd-based, Zr-based MG plates were successfully welded [11, 12, 18]. Laser additive manufacturing (LAM), such as selective laser melting (SLM) and laser foil printing (LFP), was confirmed to be a very promising method for preparing large and complex MG structures, although some issues such as cracks, crystallization, and pores still existed [14, 15, 19, 20]. By SLM, Ouyang et al. [20] successfully printed crack-free Zr-based MG composite rods with various dimensions. Using LFP as well as SLM [14, 15], three dimensional (3D) MG structures with complex geometries were built. By laser shock peening, complex residual stress could be introduced into material surface, and this method has been used to tune the plastic deformation of MGs [10, 13].

Apart from the applications of laser processing for increasing the size and plasticity of MGs, laser irradiation was also employed to fabricate micro/nanostructures on MG surface for enhancing

their functional applications as biomedical, catalytic, and hydrophobic materials. For example, by single laser pulse irradiation, surface ripples, porous nanostructures, and Saffman–Taylor fingering were observed on the irradiated surface [21-23]. Furthermore, by multi-line laser irradiation, hierarchical surface structures, i.e., laser pulse tracks covered by cotton-like MG thin film were formed [16]. Moreover, our recent studies [17, 24] showed that the surface patterns were strongly affected by the irradiation atmosphere. When laser irradiation was implemented in nitrogen shield gas, the unique cross-shaped microstructures were generated on Zr-based MG surface, and the whole surface structure significantly affected the hydrophobicity [17]. Accompanied by the appearance of cross-shaped microstructures, ZrN phase was detected on the irradiated surface. That is to say the Zr-based MG was nitrided by laser irradiation in nitrogen gas. Furthermore, the structure of materials in the laser irradiated surface is very similar to that of the so-called MG composites (MG matrix embedded with secondary phase). Previous studies commonly reported that introducing the secondary phase into the MG matrix was an effective method to improve the plasticity of MGs by impeding the propagation of single shear band and stimulating multi shear bands [6, 7, 25-27]. As laser irradiation in nitrogen gas provides a new method to introduce secondary phase into MG matrix, the effects of the formed ZrN phase (laser surface nitridation) on the mechanical properties and deformation behavior of MGs deserve further investigations, which may derive a new method for tuning mechanical characteristics of MGs.

On the other hand, some previous studies indicated that the thermal shock generated during the laser irradiation resulted in softening of MGs [28-31]. Laser surface nitriding, on the contrary, was commonly reported to harden the material surface [32, 33]. For laser irradiation of Zr-based MG in nitrogen gas, laser thermal shock and surface nitridation coexist, and their coupling effects on

mechanical properties and deformation behavior should be clarified. In this paper, by characterizing the nanoindentation response of laser irradiated Zr-based MG surface under various experimental conditions, the coupling effects of laser thermal shock and surface nitridation on indentation hardness, serrated flow, and surface shear bands were comparatively analyzed, and the underlying mechanism was further discussed.

2. Materials and methods

A typical Zr-based MG ($Zr_{41.2}Ti_{13.8}Cu_{12.5}Ni_{10}Be_{22.5}$) sample with a diameter of 10 mm and thickness of 1 mm was used in this study. Because wire electrical discharge machining (wire-EDM) was employed to cut the sample from an as-cast MG rod which resulted in rough surface as well as formation of crystalline layers [34, 35], the sample was ground by using 400, 800, and 1500 grit sand papers in sequence, and then polished by diamond abrasive paste and cleaned with alcohol. After these processes, clean and smooth MG surface was obtained for subsequent laser irradiation.

Laser irradiation was conducted by using a Nd:YAG nanosecond pulsed laser system (LR-SHG, MegaOpto Co., Ltd., Japan) (laser wavelength: 532 nm, diameter of the laser beam at focal position: ~85 μm, pulse width: 15.4 ns, and pulse frequency: 1 kHz). To introduce the ZrN phase as well as avoid oxidation, nitrogen gas with a pressure of 0.05 MPa was used as the reaction and shield gas. According to our previous research experience [17, 24], the laser irradiation conditions as listed in Table 1 were selected in this study. A fixed scanning speed of 1 mm/s was employed because the generation of ZrN phase was greatly suppressed when the scanning speed was increased to 5 or 10 mm/s [24]. Corresponding to different experimental conditions, five cases were defined, A1, A2, A3, B2, and C2. For each case, the laser beam scanned from the left to the right with a total irradiation

length of 2 mm, and 20 lines were irradiated with the corresponding overlap. To ensure the comparability of nanoindentation results, all the laser irradiation experiments were performed on the same sample with a horizontal distance of 1 mm and vertical distance of 1.5 mm between two adjacent irradiated regions. According to the experiments in Table 1, the effects of the overlap between two adjacent scanning lines, the number of irradiation cycle, and the laser power could be discussed by analyzing cases A1 and A2, A2 and A3, and A2, B2 and C2, respectively.

Table 1. Laser irradiation conditions for each case.

	Average laser power, W	Overlap, μm	Number of irradiation cycle	Scanning speed, mm/s
A1	0.580	40	1	1
A2	0.580	70	1	1
A3	0.580	70	5	1
B2	0.380	70	1	1
C2	0.180	70	1	1

After laser irradiation, the surface morphologies were observed by a scanning electron microscope (SEM) (Inspect S50, FEI, USA), and an X-ray diffractometer (XRD, D8 Discover, Bruker, Germany) was used to characterize the amorphous and crystalline features in the irradiated regions. As the MG surface became rough after laser irradiation, it was further polished by diamond abrasive paste to obtain a smooth surface for subsequent mechanical testing. The irradiated regions after polishing were further characterized by XRD, and the distribution and content of the N element as well as the MG elements were measured by energy-dispersive X-ray (EDX) spectroscopy (Bruker AXS, Germany). Then, nanoindentation tests were implemented in each irradiated regions as well as one non-irradiated region defined as case A0 by using an ENT-1100 nanoindentation instrument (Elionix Inc., Japan). The Berkovich indenter and load-control mode were used. To distinguish the effects of laser irradiation conditions (corresponding to different

contents of ZrN phase) on mechanical characteristics of MG, a constant indentation load of 100 mN and loading/unloading rate of 10 mN/s were selected according to our previous results. The holding time at the maximum indentation load was 1 s for all nanoindentation tests. For each case, 30 nanoindentation tests were done for statistic analysis. After nanoindentation testing, the residual indents were observed by a field emission scanning electron microscope (FE-SEM) (JSM-7600F, JEOL, Japan).

3. Results

Fig. 1 presents the SEM morphologies of the laser irradiated regions under different conditions. It is observed that the irradiated regions become very rough due to the strong interaction between laser and MG. At a small overlap (case A1) or a low laser power (case C2), line-like microstructures are observed, which are the so-called cross-shaped microstructures in our previous study [17]. Correspondingly, with increase in the overlap (A2) or laser power (B2), the interaction between laser and MG is greatly enhanced, resulting in the generation of a large number of nanoparticles. Thus, the irradiated regions are covered with particles. Furthermore, for the same laser power of 0.580 W (cases A2 and A3), increasing the number of irradiation cycle results in larger surface grooves. Although the interaction time between the nanosecond pulsed laser and MG is very short and the irradiated region might have cooled down prior to the next irradiation cycle, the absorption of laser energy for the irradiated region should be much higher than the polished surface because it was quite rough [36]. Accordingly, the laser-MG interaction is greatly enhanced in the subsequent irradiation cycle, resulting in larger surface grooves compared to that of single-pass irradiation.

Corresponding to the surface morphologies shown in Fig. 1, the XRD patterns are illustrated in

Fig. 2. For comparison, the XRD pattern of non-irradiated region is also given in Fig. 2(a) which shows the amorphous feature of the original sample. It is noted that crystalline peaks of ZrN phase are more or less observed in the XRD patterns obtained on the irradiated regions, whose intensity depends on the laser irradiation conditions. The comparative results in Fig. 2 show the tendency that with increase in the overlap, or the number of irradiation cycle, or the laser power, the intensity of ZrN phase is enhanced. At a relative high laser power and five times of laser irradiation, remarkable peaks of ZrN phase appear in the XRD pattern as shown in Fig. 2(d), demonstrating that more ZrN phase has been generated under this condition.

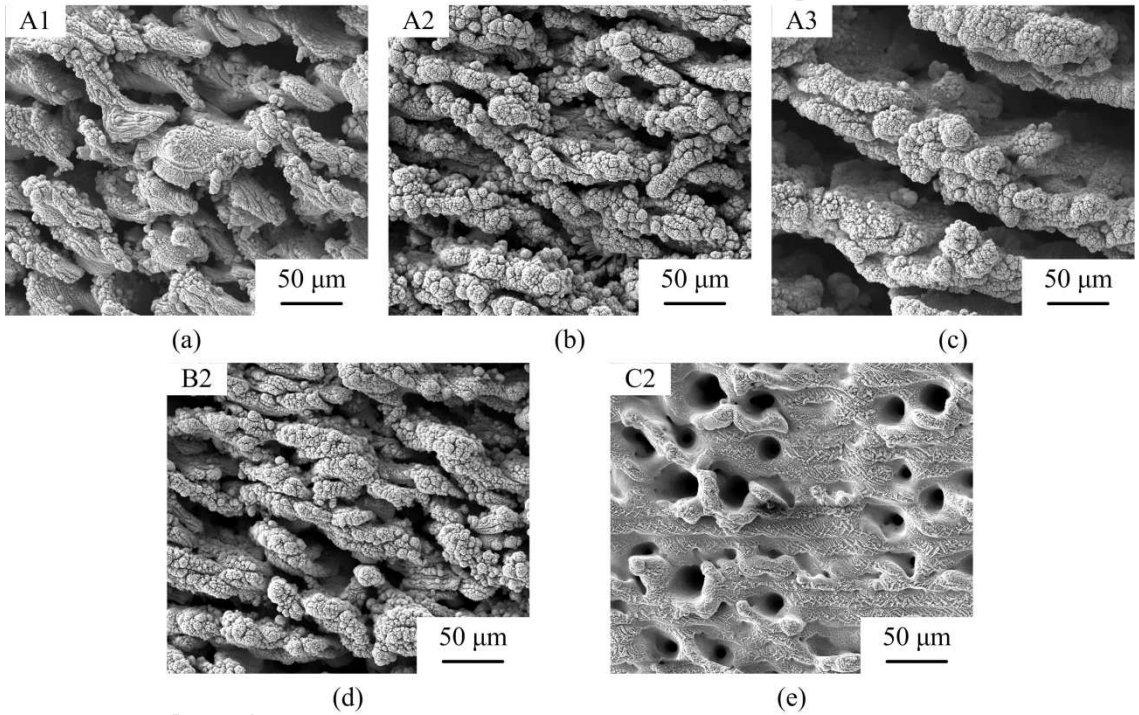

Fig. 1. SEM morphologies of the laser irradiated regions under different conditions. (a) Laser power: 0.580 W, overlap: 40 μm; (b) laser power: 0.580 W, overlap: 70 μm; (c) laser power: 0.580 W, overlap: 70 μm, irradiation cycle: 5; (d) laser power: 0.380 W, overlap: 70 μm; and (e) laser power: 0.180 W, overlap: 70 μm.

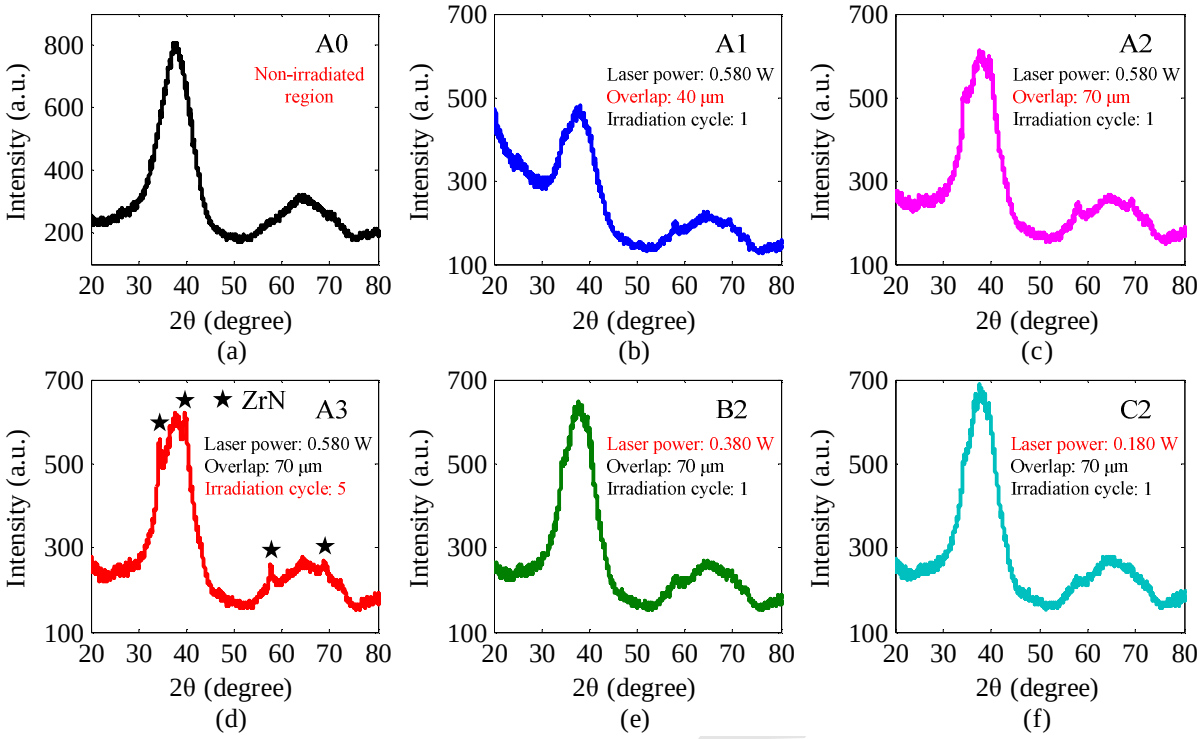

Fig. 2. XRD patterns of the laser irradiated regions under different conditions.

Fig. 3 shows the SEM morphologies of the laser irradiated regions after polishing. The surface particles and line-like microstructures shown in Fig. 1 have been removed. The polished surfaces are covered by the grooves, holes, areas and particles with very high brightness, as well as some smooth areas. The areas and particles that show very high brightness are the diamond abrasive paste which was embedded in the grooves or holes during polishing. Although the irradiated regions still seem rough after polishing, some smooth areas appear between grooves or holes, and nanoindentation tests were selected to be performed on these smooth regions.

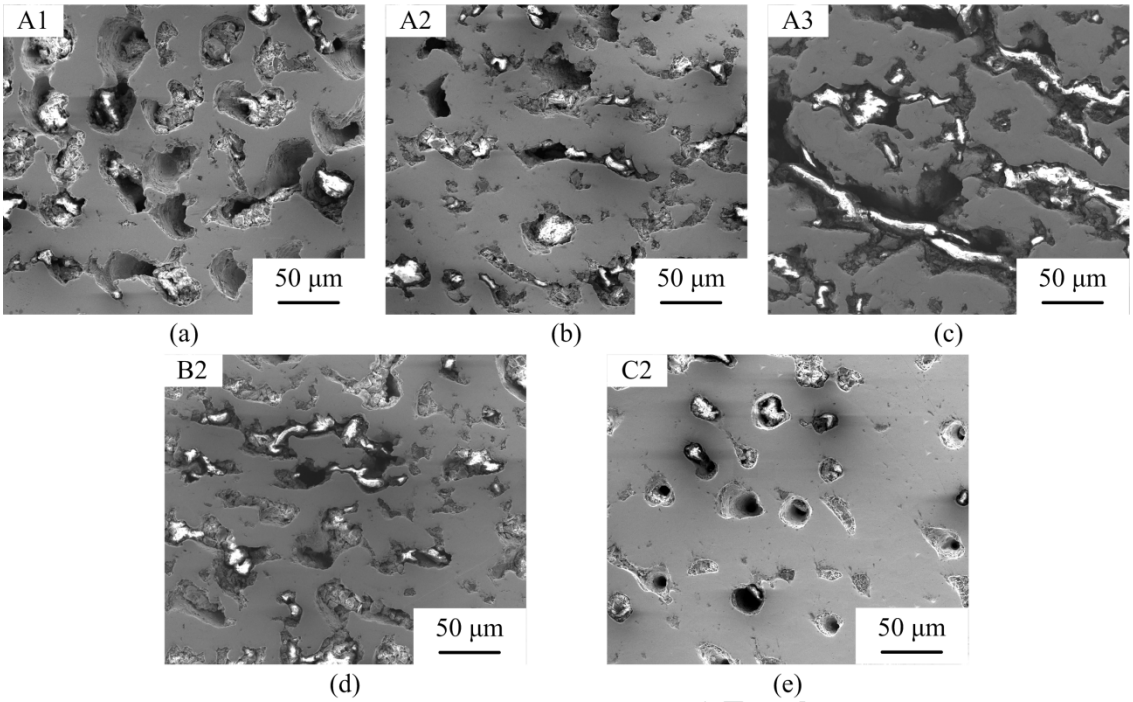

Fig. 3. SEM morphologies of the laser irradiated regions after polishing, corresponding to different conditions in Fig. 1.

To confirm that the ZrN phase was still residual in the irradiated regions after polishing, the polished regions were characterized by XRD again. The corresponding patterns are illustrated in Fig. 4 which show a very similar variation tendency to that of the XRD patterns obtained prior to polishing. The results in Fig. 4 indicate that the polished regions still contain ZrN phase and its content is different corresponding to different laser irradiation conditions. Thus, the polished sample can be employed to investigate the effects of ZrN phase on the mechanical characteristics of MG.

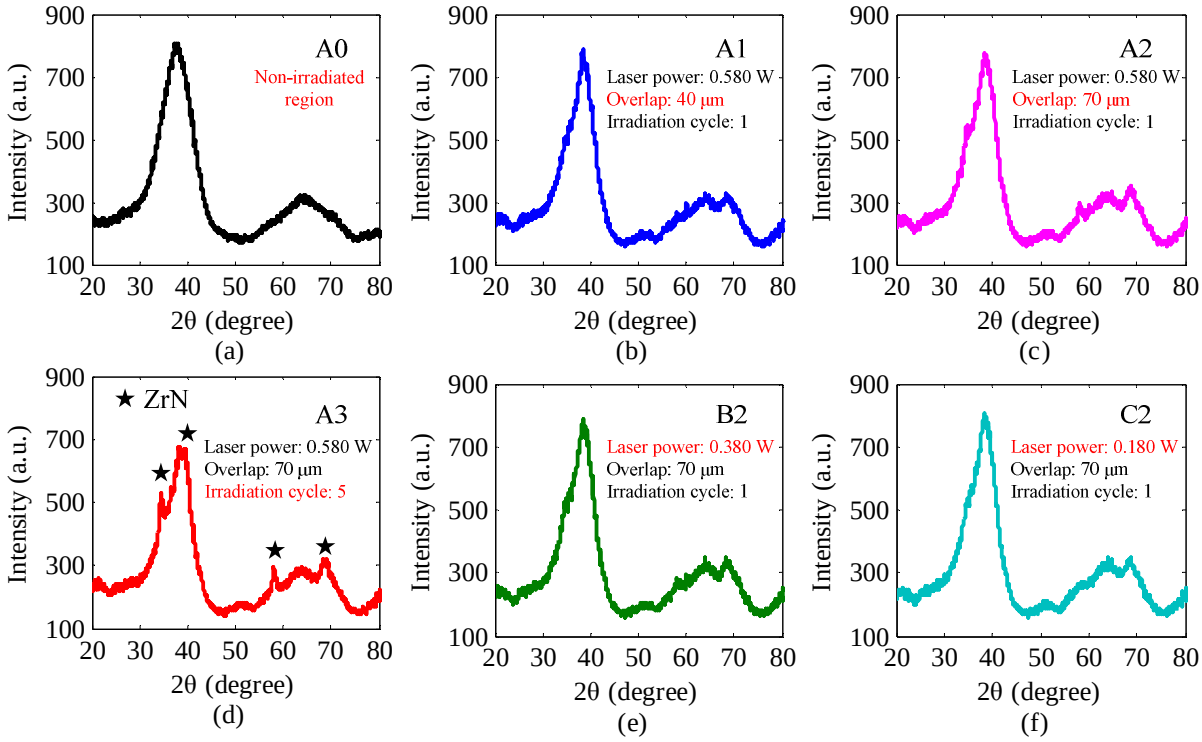

Fig. 4. XRD patterns of the laser irradiated regions after polishing, corresponding to different conditions in Fig. 2.

Fig. 5 presents the hardness distribution of different cases and the corresponding statistic results are given in Fig. 6 and Table 2. For the non-irradiated region (case A0), the hardness value is relatively stable for 30 tests and the average hardness is 6.399 GPa with a very short error bar, demonstrating that the mechanical properties of the original MG surface is relatively homogeneous. However, for the laser irradiated regions, the fluctuation of hardness value is considerably enhanced, which can be further confirmed by the large error bar and standard deviation. Especially, for case A3, the standard deviation reaches 0.668. Because grooves and holes exist in the irradiated regions, the surface roughness of the relatively smooth areas may be a little larger than that of the original surface, which could contribute to the large standard deviation in some degree. Apart from the effect of surface roughness, the introduction of ZrN phase should also have significantly affected the hardness distribution because the variation tendency of the standard deviation is very similar to that

of the intensity of ZrN phase for various cases, i.e., the higher the intensity, the larger the standard deviation.

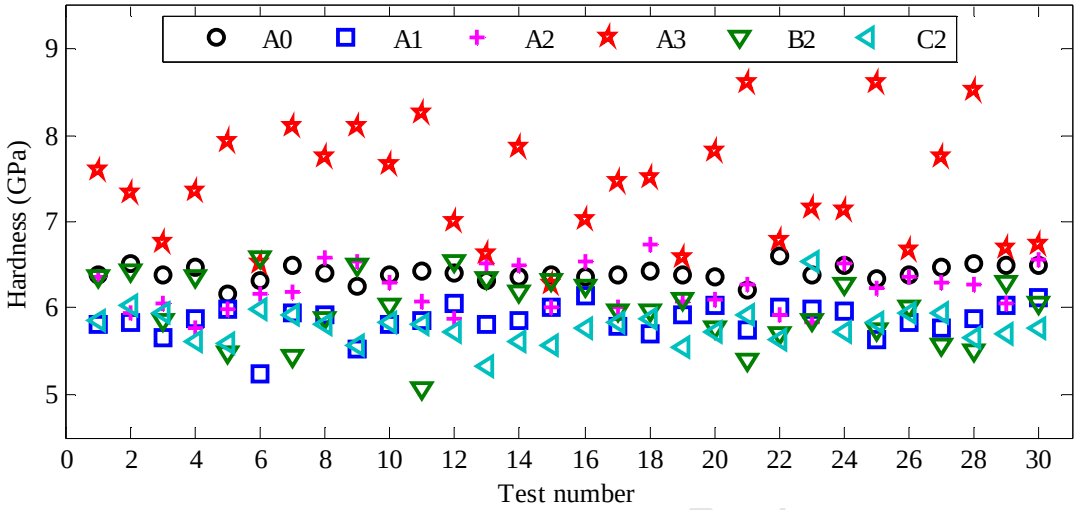

Figure 5. Hardness distribution of different cases (30 tests).

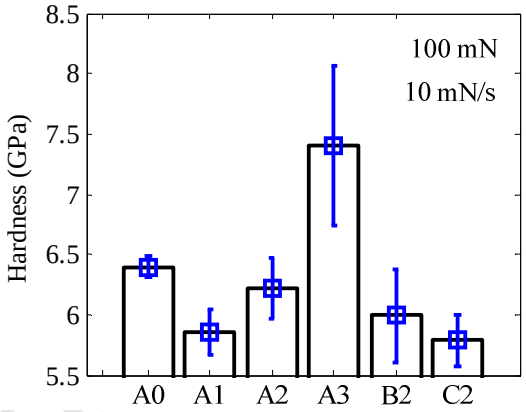

Fig. 6. Hardness values for different samples.

Table 2. Statistical results of hardness (30 nanoindentation tests for each case).

	A0	A1	A2	A3	B2	C2
Average hardness, GPa	6.399	5.858	6.219	7.403	5.993	5.785
Standard deviation, GPa	0.093	0.186	0.258	0.668	0.387	0.213

On the other hand, for cases A1, A2, B2, and C2, the average hardness is less than that of the original MG surface (case A0), showing surface softening especially for cases A1 and C2. Furthermore, from case A1 to case A2, the average hardness tends to gradually increase, and similar

change occurs from case C2 to case B2. Being different from aforementioned cases, the average hardness of case A3 reaches 7.403 GPa, which is significantly higher than those of all the other cases including the original MG surface, showing surface hardening. Moreover, although the hardness value for case A3 is quite scattered as shown in Fig. 5, the measured minimum value for case A3 is almost the same to the maximum value obtained on the original MG surface (case A0), and the maximum value for case A3 reaches 8.606 GPa which is 2.207 GPa higher than that of the average value for case A0.

As significant change in indentation hardness has been observed, the micro-scale plastic deformation of MG might have been significantly affected as well. This kind of effects can be investigated by analyzing the discontinuous depth bursts in the load-depth curve, i.e., the so-called serrated flow in the field of MG [37]. Figs. 7(a), (c), (e), (g), (i), and (k) show the representative load-depth curves corresponding to cases A0, A1, A2, A3, B2, and C2 respectively, and the inserted figures are the local enlarged views in the load range of 70-100 mN showing the serrated flow in detail. To further highlight the serrated flow in the entire range of the indentation load, the depth-difference method was employed [38] and the corresponding depth difference-load curves are illustrated in Figs. 7(b), (d), (f), (h), (j), and (l), respectively. One sharp peak in the depth difference-load curve denotes one serrated flow in the loading curve, and the higher the peak, the larger the serrated flow. From the depth difference-load curve, the number and intensity of the serrated flow could be comparatively analyzed easily. In Figs. 7(a) and 7(b), for the original MG surface (case A0), serrated flows are uniformly distributed in this loading curve, resulting in stair-step shape of the loading curve and many sharp peaks in the depth difference-load curve. Compared to the case A0, the number of serrated flows is gradually decreased from case A1 to case

A3, and the loading curve becomes almost smooth without visible serrated flow for case A3. However, from cases A2 to B2 and further to C2, the number of serrated flow tends to increase. The results in Fig. 7 indicate that the serrated flows have been significantly affected by the processing of laser irradiation in nitrogen gas, suggesting the change in plastic deformation of MG.

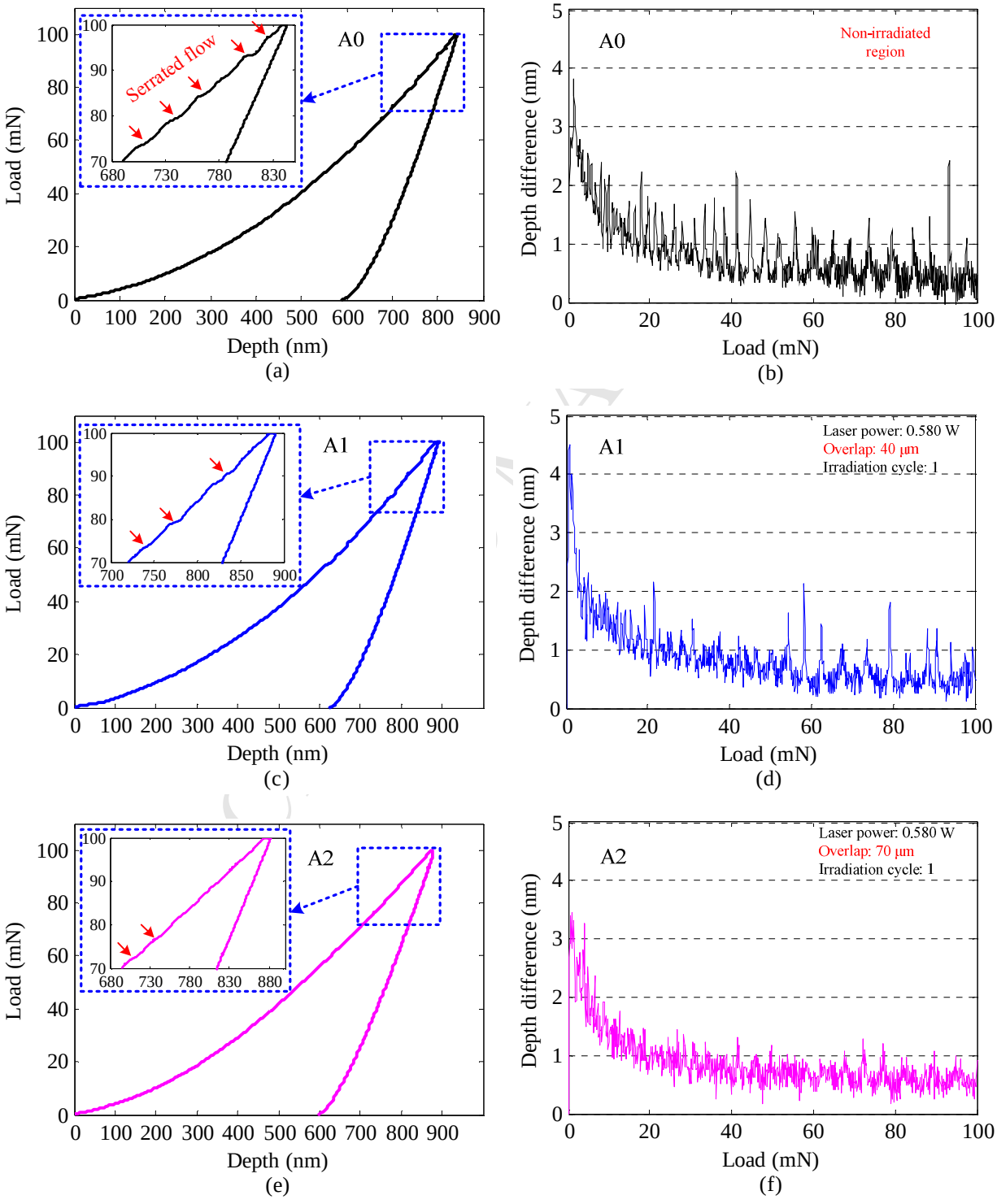

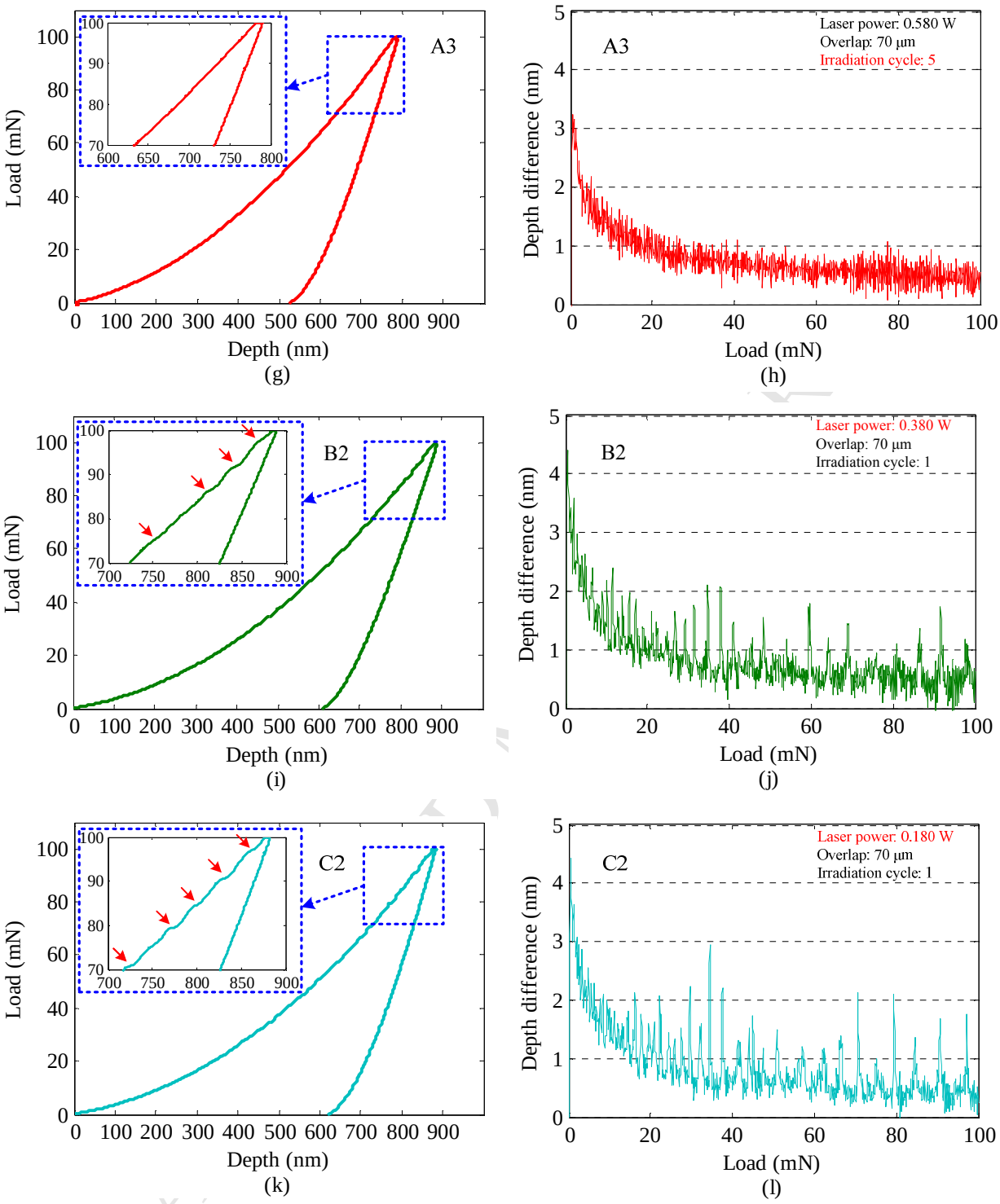

Fig. 7. Representative load-depth curves and corresponding depth difference-load curves: (a) and (b): case A0, (c) and (d): case A1, (e) and (f): case A2, (g) and (h): case A3, (i) and (j): case B2, (k) and (l): case C2.

Shear banding is regarded as the main plastic deformation mechanism in MG, which eventually evolves to be macroscopic shear bands inside and on the surface of MG sample [39, 40]. It is commonly accepted that serrated flows are directly related to the operations of shear bands [37, 41], for example nucleation, propagation, and arrest of shear bands. The evolution of serrated flows suggests that the shear bands around the residual indents should also have been affected by the laser irradiation conditions. To confirm this effect, the representative SEM morphologies of residual indents are presented in Fig. 8. Because the variation tendency of serrated flows from cases A0 to A1, A2, and A3 is very similar to that from cases A0 to C2, B2, and A2, the SEM morphologies of residual indents obtained from cases A0 to A1, A2, and A3 are given as example. In Fig. 8(a), semicircle shear bands are observed around the residual indent, being consistent with the large number of serrated flows in Figs. 7(a) and 7(b). It is further noted that the number of surface shear bands gradually decreases from cases A0 to A1, A2, and A3, and there is nearly no visible surface shear bands around the residual indent obtained from case A3. This variation tendency agrees well with the evolution of serrated flows for these cases. On the other hand, as the SEM images in Fig. 7 are measured with the same magnification, the indent size for case A0, A1, and A2 shows no big difference, but they are obviously larger than that for case A3. This fact further confirms the hardening role under case A3.

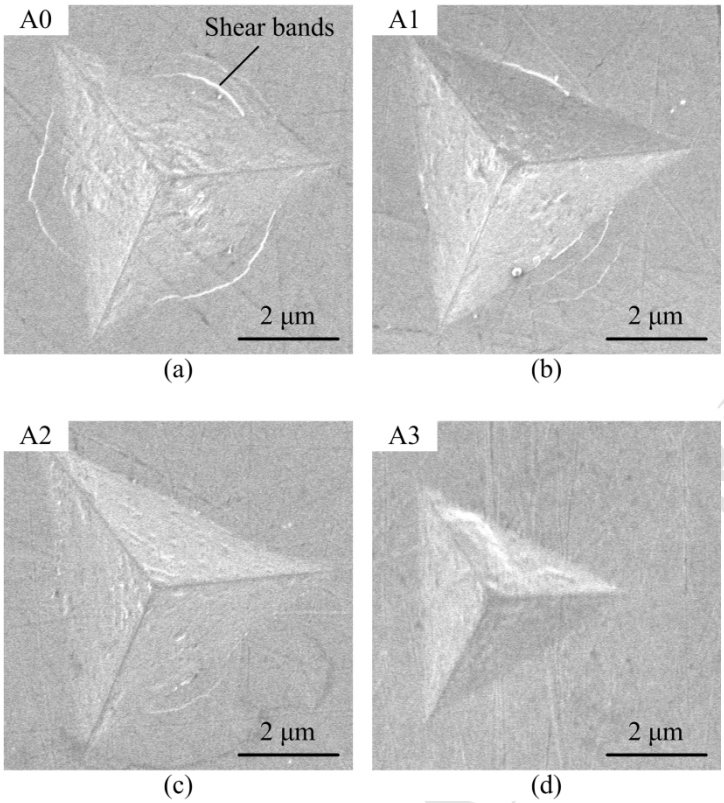

Fig. 8. Representative SEM morphologies of the residual indents for (a) case A0, (b) case A1, (c) case A2, and (d) case A3.

4. Discussion

From abovementioned experimental results, it can be concluded that laser irradiation in nitrogen gas has significantly affected the surface mechanical properties and deformation behavior of Zr-based MG. Table 3 summarizes the variation tendency of characteristics under different cases and the numbers 1 to 4 denote different levels from low to high. As the variation tendency from cases A1 to A2 and further to A3 is very similar to that from cases C2 to B2 and further to A3, only the comparative analysis between A0 to A3 will be conducted for simplicity.

Table 3. Variation tendency of characteristics under different cases. The numbers 1 to 4 denote different levels: 1 low and 4 high.

Case	Average hardness	Number of serrated flow	Surface shear bands

A0	3	4	4
A1	1	3	3
A2	2	2	2
A3	4	1	1

In Table 3, from cases A0 to A3, both the number of serrated flows and surface shear bands decrease, but the change in average hardness does not show similar variation tendency which first decreases and then increases. Nevertheless, by analyzing cases A1 to A3, the rule could be obtained that with increase in average hardness, both the number of serrated flows and surface shear bands decrease. In previous studies [28-31], decrease in surface hardness of MG was reported after laser irradiation in non-nitrogen gas, which means that laser thermal shock could only result in surface softening. However, in the current study, the average hardness for case A3 is significantly higher than that of case A0. If the decrease in average hardness for cases A1 and A2 could be caused by the laser thermal shock, the increase in hardness for case A3 should result from some other reasons. Compared to previous studies, the main difference in the current study is the introduction of ZrN phase by laser irradiation in nitrogen gas, which should be the main reason leading to surface hardening for case A3. The regular variation tendency of characteristics from cases A1 to A3 may confirm the role of ZrN phase.

To further verify this deduction, the contents of ZrN phase for cases A1 to A3 were evaluated by measuring the content of N element in the irradiated region through EDX mapping with sampling time of 25 minutes. Taking case A2 for example, Fig. 9 presents the distribution of elements in the mapping region. Because Be element is a light chemical element, it was not measured here. From Figs. 9(b) to 9(f), it is observed that the distribution of MG elements (Zr, Ti, Cu, and Ni) as well as N element is quite uniform, which indicates that no phase separation and element enrichment occur under the current irradiation condition. For cases A1, A2, and A3, the

quantitative statistic results of each element are listed in Table 4 by means of atomic percent. It is clear that from cases A1 to A3, the content of N element tends to increase, being consistent with the variation tendency of peak intensity of ZrN phase in the XRD patterns shown in Figs. 4(b) to 4(d).

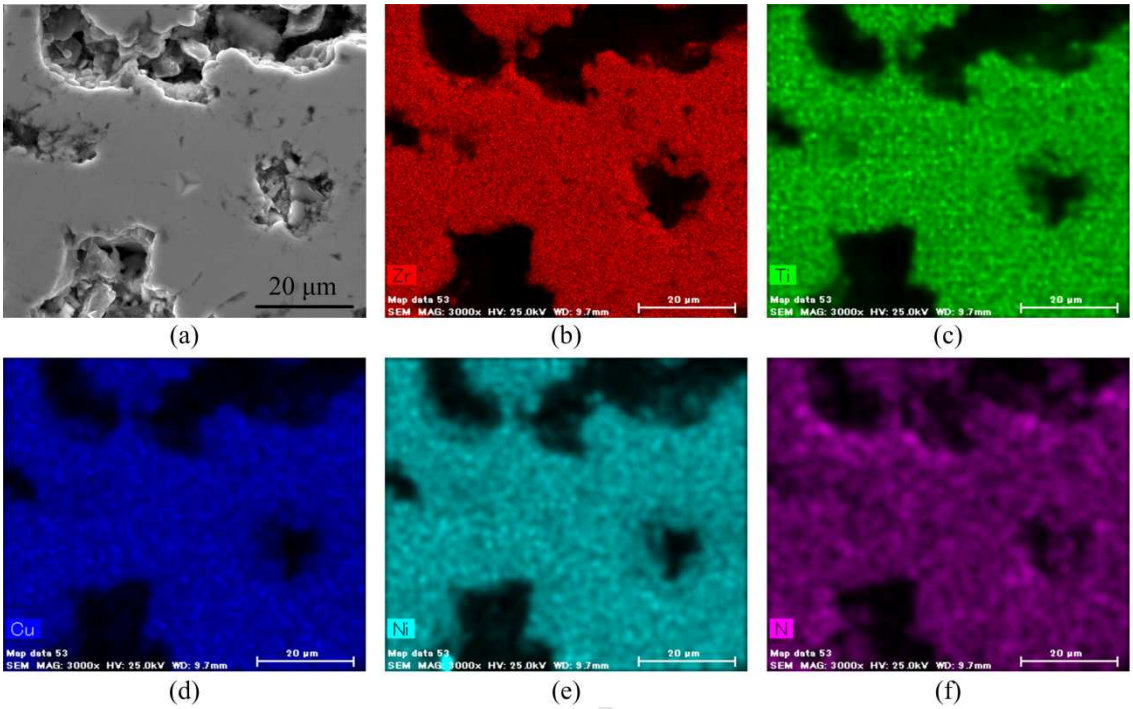

Fig. 9. Results of EDX mapping for case A2: (a) the mapping region, (b) Zr, (c) Ti, (d) Cu, (e) Ni, and (f) N.

Table 4. Atomic percent of each element obtained for cases A1, A2, and A3.

Case	Zr	Ti	Cu	Ni	N
A3	49.23	14.05	13.75	10.25	12.72
A2	49.08	15.32	16.06	11.94	7.60
A1	49.86	15.61	16.44	12.02	6.07

Now, the effects of laser irradiation in nitrogen gas on the mechanical properties and deformation behavior could be explained by the coupling role of laser thermal shock and ZrN phase (surface nitridation). Laser thermal shock was reported to result in the generation of free volume and pre-existing shear bands [28, 30, 31, 42]. Whatever the specific reason is, both of them have the role to soften the MG surface, i.e., laser thermal shock softens the MG surface. On the contrary, the introduction of ZrN phase impedes the propagation of single shear band and hence increases the

resistance of plastic deformation, playing the role of hardening the MG surface. Moreover, ZrN phase itself has a much higher hardness than MG, further contributing to the increase in surface hardness. Accordingly, the final hardness is determined by the coupling roles of laser thermal shock and ZrN phase. If the content of ZrN phase is low, the softened role by laser thermal shock is dominant, and thus low hardness but relatively more serrated flows and surface shear bands appear, typically for example case A1; while, if the content of ZrN phase is high, the hardened role of ZrN phase is dominant, resulting in increased hardness but relatively less serrated flows and surface shear bands, typically for example case A3. Overall, laser irradiation of Zr-based MG in nitrogen gas provides a new method to introduce secondary phase into the MG surface, which has been confirmed that has the role to tune the surface mechanical characteristics of MG. Alike Zr element, Ti element also has strong affinity with N element, therefore this method could be available for Ti-based MG as well, which will be attempted in our future study.

The above results and discussion are performed in the horizontal plane, and the distribution of ZrN phase along the depth direction is also a focusing point. For this purpose, EDX line scan was employed to measure the element content along the depth direction. Because the irradiated surfaces obtained under the above used experimental conditions are very rough and wrinkled, being difficult to identify the top surface, some other experimental parameters were selected according to our previous study (average laser power: 0.148 W, scanning speed: 1 mm/s, the number of irradiation cycle: 1, and overlap: 70 and 40 μm for comparison) [17]. The irradiated regions were cut by a low speed diamond saw and the cross-sections were ground and polished for EDX measurement. The results corresponding to overlaps of 70 and 40 μm are presented in Figs. 10 and 11, respectively. The point 1 in these two figures denotes the measuring origination, which is very close to the top

surface. In Fig.10, it is noted that the contents of N and Zr elements show similar variation tendency, first increase, then decrease, then increase again, and finally decrease to a stable value. This variation process indicates that ZrN phase is enriched in two layer, the top surface and the subsurface layer with a certain distance to the top surface. The subsurface layer is formed between two interactive interface when the adjacent laser irradiation overlaps the preceding irradiated region where ZrN phase has been generated on the surface. In Fig. 10, when the overlap is 70 μm, the depth of the affecting layer by ZrN phase reaches 8.3 μm. However, when the overlap is decreased to 40 μm, only one enriched peak appears in Fig. 11 and the corresponding depth of the affecting layer is decreased to 3.3 μm as well. Here, we just give an example showing the distribution of ZrN phase along the depth direction. According to the XRD patterns in Fig. 2, it could be derived that with increase in the laser power, the overlap, and the number of irradiation cycle, the depth of affecting layer by ZrN phase should increase. Thus, for specific requirements, the laser irradiation conditions should be optimized.

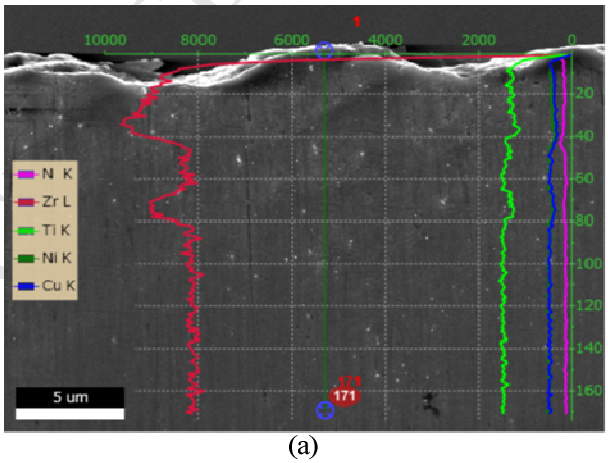

(a)

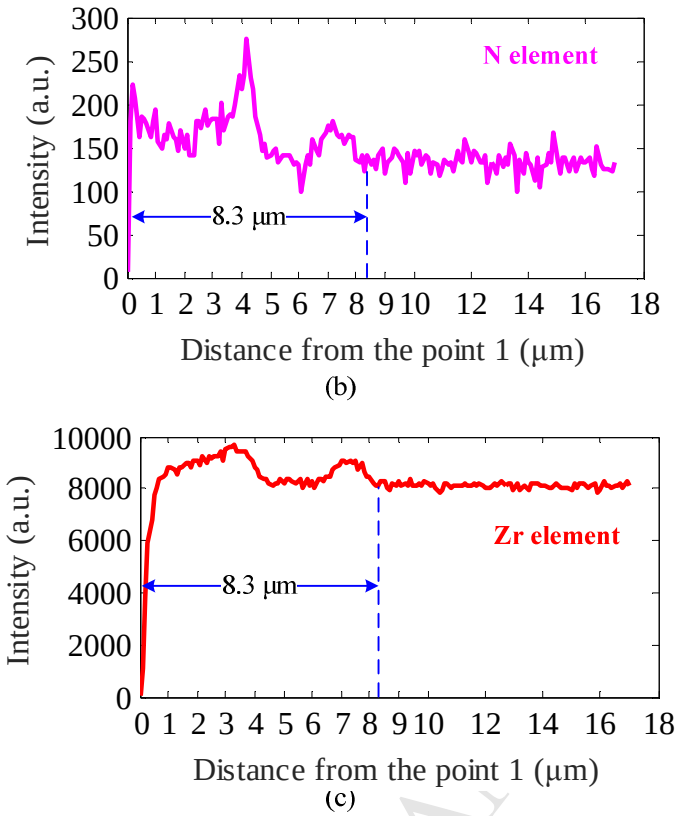

Fig. 10. Results of EDX line scan measured on the cross-section (average laser power: 0.148 W, scanning speed: 1 mm/s, the number of irradiation cycle: 1, and overlap: 70 μm).

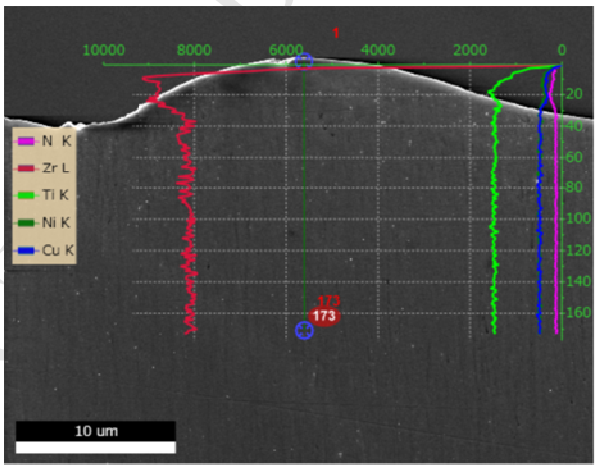

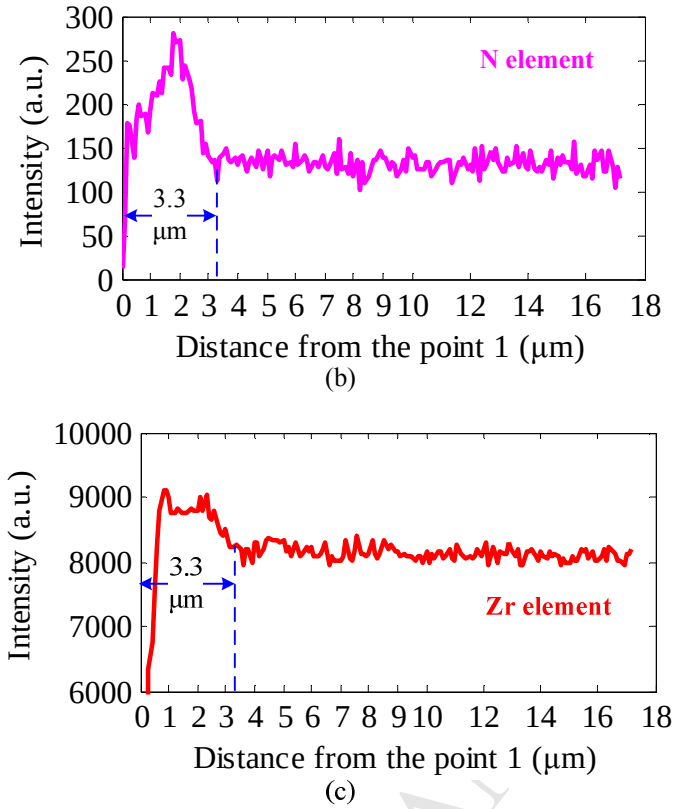

Fig. 11. Results of EDX line scan measured on the cross-section (average laser power: 0.148 W, scanning speed: 1 mm/s, the number of irradiation cycle: 1, and overlap: 40 μm).

5. Conclusions and Outlook

In this study, the effects of laser irradiation in nitrogen gas on the mechanical properties and deformation behavior of Zr-based MG were investigated. From experiments and analysis, the following conclusions could be obtained.

(1) The ZrN phase was generated in the Zr-based MG matrix after laser irradiation in nitrogen gas and its content strongly depended on the laser irradiation conditions. With increase in the laser power, the overlap, and the number of irradiation cycle, the content of ZrN phase tended to increase.

(2) The nanoindentation hardness, serrated flow, and surface shear bands were significantly affected

by laser irradiation in nitrogen gas, which could be ascribed to the coupling roles of laser thermal shock and the introduction of ZrN phase (surface nitridation). Their competition relationship determined the final surface mechanical characteristics. In general, if the content of ZrN phase was low, the softened role by laser thermal shock was dominant, resulting in low hardness but relatively more serrated flows and surface shear bands; while, if the content of ZrN phase was high, the hardened role of ZrN phase was dominant, resulting in increased hardness but relatively less serrated flows and surface shear bands.

(3) As an example, the affecting layer of ZrN phase was evaluated by EDX line scan under two different overlaps. It showed that the distribution of ZrN phase along the depth direction and the depth of affecting layer were affected by the laser irradiation conditions.

The above results suggest that laser irradiation in nitrogen gas may provide a new method to introduce secondary phase into Zr-based MG surface and further to tune its surface mechanical properties and deformation behavior. As fundamental research in the current study, the laser irradiation parameters are not optimized, and thus, some of the irradiated surfaces here are quite rough. For practical applications, the following optimization methods could be employed to produce smoother irradiated surface: (1) use a low laser power and increase the pressure of nitrogen gas, (2) use a low laser power and increase the number of irradiation cycle, (3) use a relatively high laser power and increase the scanning speed, (4) optimize the path of laser irradiation, et al.

On the other hand, as ZrN phase has been generated into the MG matrix, the crystallographic and interface characteristics between ZrN phase and amorphous phase should be an interesting topic, which will be further investigated by high resolution microscopic analysis such as transmission electron microscope (TEM) in our future work.

Acknowledgement

This work was supported by the National Natural Science Foundation of China (Grant No. 51705197, 11522221), Opening fund of State Key Laboratory of Nonlinear Mechanics (Grant No. LNM201802), Young Elite Scientists Sponsorship Program by CAST(YESS) (Grant No. 2017QNRC001), the Fundamental Research Funds for the Central Universities, and Grant-in-Aid for JSPS Fellows (Grant No. 26-04048).

References

[1] M.M. Khan, A. Nemati, Z.U. Rahman, U.H. Shah, H. Asgar, W. Haider, Recent advancements in bulk metallic glasses and their applications: A review, Crit. Rev. Solid State Mater. Sci. 43(3) (2018) 233-268.
[2] W.H. Wang, The elastic properties, elastic models and elastic perspectives of metallic glasses, Prog. Mater. Sci. 57(3) (2012) 487-656.
[3] J. Plummer, W.L. Johnson, Is metallic glass poised to come of age?, Nat. Mater. 14(6) (2015) 553-555.
[4] M. Telford, The case for bulk metallic glass, Mater. Today 7(3) (2004) 36-43.
[5] J. Schroers, BULK Metallic Glasses, Phys. Today 66(2) (2013) 32-37.
[6] J.W. Qiao, H.L. Jia, P.K. Liaw, Metallic glass matrix composites, Mater. Sci. Eng., R 100 (2016) 1-69.
[7] C.C. Hays, C.P. Kim, W.L. Johnson, Microstructure controlled shear band pattern formation and enhanced plasticity of bulk metallic glasses containing in situ formed ductile phase dendrite dispersions, Phys. Rev. Lett. 84(13) (2000) 2901-2904.
[8] M.H. Lee, K.S. Lee, J. Das, J. Thomas, U. Kuhn, J. Eckert, Improved plasticity of bulk metallic glasses upon cold rolling, Scr. Mater. 62(9) (2010) 678-681.
[9] W.M. Yang, H.S. Liu, Y.C. Zhao, A. Inoue, K.M. Jiang, J.T. Huo, H.B. Ling, Q. Li, B.L. Shen, Mechanical properties and structural features of novel Fe-based bulk metallic glasses with unprecedented plasticity, Sci. Rep. 4 (2014) 6233.
[10] M. Liang, Y.H. Zhu, Z. Ji, J. Fu, C. Zheng, Effect of laser shock peening and its size-dependence on the compressive plasticity of Zr-based bulk metallic glass, J. Mater. Process. Technol. 251 (2018) 47-53.
[11] G. Wang, Y.J. Huang, M. Shagiev, J. Shen, Laser welding of Ti40Zr25Ni3Cu12Be20 bulk metallic glass, Mater. Sci. Eng., A 541 (2012) 33-37.
[12] B.A. Chen, T.L. Shi, M. Li, Z.B. Zhang, Z.J. Zhu, G.L. Liao, Laser Welding of Zr41Ti14Cu12Ni10Be23 Bulk Metallic Glass: Experiment and Temperature Field Simulation, Adv. Eng. Mater. 15(5) (2013) 407-413.
[13] J. Fu, Y.H. Zhu, C. Zheng, R. Liu, Z. Ji, Effect of laser shock peening on the compressive deformation and plastic behavior of Zr-based bulk metallic glass, Opt. Lasers Eng. 86 (2016) 53-61.
[14] Y.Y. Shen, Y.Q. Li, C. Chen, H.L. Tsai, 3D printing of large, complex metallic glass structures, Mater. Des. 117 (2017) 213-222.
[15] C. Yang, C. Zhang, W. Xing, L. Liu, 3D printing of Zr-based bulk metallic glasses with complex geometries and enhanced catalytic properties, Intermetallics 94 (2018) 22-28.

[16] H. Huang, N. Jun, M.Q. Jiang, M. Ryoko, J.W. Yan, Nanosecond pulsed laser irradiation induced hierarchical micro/nanostructures on Zr-based metallic glass substrate, Mater. Des. 109 (2016) 153-161.

[17] H. Huang, J.W. Yan, Surface patterning of Zr-based metallic glass by laser irradiation induced selective thermoplastic extrusion in nitrogen gas, J. Micromech. Microeng. 27(7) (2017) 075007.

[18] L. Shao, A. Datye, J.K. Huang, J. Ketkaew, S.W. Sohn, S.F. Zhao, S.J. Wu, Y.M. Zhang, U.D. Schwarz, J. Schroers, Pulsed Laser Beam Welding of Pd43Cu27Ni10P20 Bulk Metallic Glass, Sci. Rep. 7 (2017) 7989.

[19] N. Li, J.J. Zhang, W. Xing, D. Ouyang, L. Liu, 3D printing of Fe-based bulk metallic glass composites with combined high strength and fracture toughness, Mater. Des. 143 (2018) 285-296.

[20] D. Ouyang, N. Li, W. Xing, J.J. Zhang, L. Liu, 3D printing of crack-free high strength Zr-based bulk metallic glass composite by selective laser melting, Intermetallics 90 (2017) 128-134.

[21] Y. Liu, M.Q. Jiang, G.W. Yang, Y.J. Guan, L.H. Dai, Surface rippling on bulk metallic glass under nanosecond pulse laser ablation, Appl. Phys. Lett. 99(19) (2011) 191902.

[22] M.Q. Jiang, Y.P. Wei, G. Wilde, L.H. Dai, Explosive boiling of a metallic glass superheated by nanosecond pulse laser ablation, Appl. Phys. Lett. 106(2) (2015) 021904.

[23] Y. Liu, M.Q. Jiang, G.W. Yang, J.H. Chen, Y.J. Guan, L.H. Dai, Saffman-Taylor fingering in nanosecond pulse laser ablating bulk metallic glass in water, Intermetallics 31 (2012) 325-329.

[24] H. Huang, J. Noguchi, J.W. Yan, Shield gas induced cracks during nanosecond-pulsed laser irradiation of Zr-based metallic glass, Appl. Phys. A-Mater. 122(10) (2016) 881.

[25] Z.L. Ning, W.Z. Liang, M.X. Zhang, Z.Z. Li, H.C. Sun, A.L. Liu, J.F. Sun, High tensile plasticity and strength of a CuZr-based bulk metallic glass composite, Mater. Des. 90 (2016) 145-150.

[26] J.L. Cheng, G. Chen, W. Zhao, Z.Z. Wang, Z.W. Zhang, Enhancement of tensile properties by the solid solution strengthening of nitrogen in Zr-based metallic glass composites, Mater. Sci. Eng., A 696 (2017) 461-465.

[27] X.F. Liu, Y. Chen, M.Q. Jiang, P.K. Liaw, L.H. Dai, Tuning plasticity of in-situ dendrite metallic glass composites via the dendrite-volume-fraction-dependent shear banding, Mater. Sci. Eng., A 680 (2017) 121-129.

[28] Y.H. Zhu, J. Fu, C. Zheng, Z. Ji, Effect of laser shock peening without absorbent coating on the mechanical properties of Zr-based bulk metallic glass, Opt. Laser Technol. 75 (2015) 157-163.

[29] Y.H. Zhu, J. Fu, C. Zheng, Z. Ji, Structural and mechanical modifications induced on Zr-based bulk metallic glass by laser shock peening, Opt. Laser Technol. 86 (2016) 54-60.

[30] L. Wang, L. Wang, Y.F. Xue, H.F. Zhang, H.M. Fu, Nanoindentation response of laser shock peened Ti-based bulk metallic glass, Aip Advances 5(5) (2015) 057156.

[31] H. Huang, M.Q. Jiang, J.W. Yan, Softening of Zr-based metallic glass induced by nanosecond pulsed laser irradiation, J. Alloys Compd. 754 (2018) 215-221.

[32] H. Mohseni, P. Nandwana, A. Tsoi, R. Banerjee, T.W. Scharf, In situ nitrided titanium alloys: Microstructural evolution during solidification and wear, Acta Mater. 83 (2015) 61-74.

[33] D. Hoche, P. Schaaf, Laser nitriding: investigations on the model system TiN. A review, Heat Mass Transfer. 47(5) (2011) 519-540.

[34] H. Huang, J.W. Yan, On the surface characteristics of a Zr-based bulk metallic glass processed by microelectrical discharge machining, Appl. Surf. Sci. 355 (2015) 1306-1315.

[35] H. Huang, J.W. Yan, Microstructural changes of Zr-based metallic glass during microelectrical discharge machining and grinding by a sintered diamond tool, J. Alloys Compd. 688 (2016) 14-21.

[36] D. Bergstrom, J. Powell, A.F.H. Kaplan, The absorption of light by rough metal surfaces - A three-dimensional ray-tracing analysis, J. Appl. Phys. 103(10) (2008) 103515.

[37] C.A. Schuh, T.C. Hufnagel, U. Ramamurty, Overview No.144 - Mechanical behavior of amorphous alloys, Acta Mater. 55(12) (2007) 4067-4109.

[38] H. Huang, H.W. Zhao, Z.Y. Zhang, Z.J. Yang, Z.C. Ma, Influences of sample preparation on nanoindentation behavior of a Zr-based bulk metallic glass, Materials 5(6) (2012) 1033-1039.

[39] A.L. Greer, Y.Q. Cheng, E. Ma, Shear bands in metallic glasses, Mater. Sci. Eng., R 74(4) (2013) 71-132.

[40] T.C. Hufnagel, C.A. Schuh, M.L. Falk, Deformation of metallic glasses: Recent developments in theory, simulations, and experiments, Acta Mater. 109 (2016) 375-393.

[41] H. Huang, J.W. Yan, Investigating shear band interaction in metallic glasses by adjacent nanoindentation, Mater. Sci. Eng., A 704 (2017) 375-385.

[42] Y.F. Cao, X. Xie, J. Antonaglia, B. Winiarski, G. Wang, Y.C. Shin, P.J. Withers, K.A. Dahmen, P.K. Liaw, Laser Shock Peening on Zr-based Bulk Metallic Glass and Its Effect on Plasticity: Experiment and Modeling, Sci. Rep. 5 (2015) 10789.

Figure captions

Fig. 1. SEM morphologies of the laser irradiated regions under different conditions. (a) Laser power: 0.580 W, overlap: 40 μm; (b) laser power: 0.580 W, overlap: 70 μm; (c) laser power: 0.580 W, overlap: 70 μm, irradiation cycle: 5; (d) laser power: 0.380 W, overlap: 70 μm; and (e) laser power: 0.180 W, overlap: 70 μm.

Fig. 2. XRD patterns of the laser irradiated regions under different conditions.

Fig. 3. SEM morphologies of the laser irradiated regions after polishing, corresponding to different conditions in Fig. 1.

Fig. 4. XRD patterns of the laser irradiated regions after polishing, corresponding to different conditions in Fig. 2.

Fig. 5. Hardness distribution of different cases (30 tests).

Fig. 6. Hardness values for different samples.

Fig. 7. Representative load-depth curves and corresponding depth difference-load curves: (a) and (b): case A0, (c) and (d): case A1, (e) and (f): case A2, (g) and (h): case A3, (i) and (j): case B2, (k) and (l): case C2.

Fig. 8. Representative SEM morphologies of the residual indents for (a) case A0, (b) case A1, (c) case A2, and (d) case A3.

Fig. 9. Results of EDX mapping for case A2: (a) the mapping region, (b) Zr, (c) Ti, (d) Cu, (e) Ni, and (f) N.

Fig. 10. Results of EDX line scan measured on the cross-section (average laser power: 0.148 W, scanning speed: 1 mm/s, the number of irradiation cycle: 1, and overlap: 70 μm).

Fig. 11. Results of EDX line scan measured on the cross-section (average laser power: 0.148 W, scanning speed: 1 mm/s, the number of irradiation cycle: 1, and overlap: 40 μm).

Highlights:

1. Mechanical properties of MG were tuned by laser irradiation in nitrogen gas.
2. Both surface softening and hardening were observed.
3. The hardness, serrated flow, and shear bands were significantly affected.
4. The coupling effects of laser thermal shock and surface nitridation were discussed.